

Particle Flow Calorimetry at the ILC*

M. A. Thomson¹

¹Dept. of Physics, Cavendish Laboratory, Univ. of Cambridge, JJ Thomson Av., Cambridge CB3 0HE, UK
(Dated: November 13, 2018)

One of the most important requirements for a detector at the ILC is good jet energy resolution. It is widely believed that the particle flow approach to calorimetry is the key to achieving the goal of $0.3/\sqrt{E(\text{GeV})}$. This paper describes the current performance of the PANDORAPFA particle flow algorithm. For 45 GeV jets in the Tesla TDR detector concept, the ILC jet energy resolution goal is reached. At higher energies the jet energy resolution becomes worse and can be described by the empirical expression: $\sigma_E/E \approx 0.265/\sqrt{E(\text{GeV})} + 1.2 \times 10^{-4}E(\text{GeV})$.

PACS numbers: 07.05.Kf, 29.40.Vj, 29.85.+c

Keywords: calorimetry, particle flow

I. INTRODUCTION

Many of the interesting physics processes at the ILC will be characterised by multi-jet final states, often accompanied by charged leptons and/or missing transverse energy associated with neutrinos or the lightest super-symmetric particles. The reconstruction of the invariant masses of two or more jets will provide a powerful tool for event reconstruction and identification. Unlike at LEP, where kinematic fitting[1] enabled precise jet-jet invariant mass reconstruction almost independent of the jet energy resolution, at the ILC this mass reconstruction will rely on the detector having excellent jet energy resolution. The ILC goal is to achieve a mass resolution for $W \rightarrow q/\bar{q}$ and $Z \rightarrow q\bar{q}$ decays which is comparable to their natural widths, i.e. ~ 2 GeV. A jet energy resolution of $\sigma_E/E = \alpha/\sqrt{E(\text{GeV})}$ leads to a di-jet mass resolution of roughly $\sigma_m/m = \alpha/\sqrt{E_{jj}(\text{GeV})}$, where E_{jj} is the energy of the di-jet system. At the ILC typical di-jet energies will be in the range 150 – 350 GeV, suggesting the goal of $\sigma_E/E = 0.3/\sqrt{E(\text{GeV})}$. This is more than a factor two better than the best jet energy resolution achieved at LEP, $\sigma_E/E = 0.6(1 + |\cos \theta|)/\sqrt{E(\text{GeV})}$ [2]. Meeting the jet energy resolution goal is a major factor in the overall design of a detector for the ILC.

II. THE PARTICLE FLOW APPROACH TO CALORIMETRY

It is widely believed that the most promising strategy for achieving a jet energy resolution of $\sigma_E/E = 0.30/\sqrt{E(\text{GeV})}$ at the ILC is the particle flow analysis (PFA) approach to calorimetry. In contrast to a purely calorimetric measurement, particle flow requires the reconstruction of the four-vectors of all visible particles in an event. The reconstructed jet energy is the sum of the energies of the individual particles. The momenta of charged particles are measured in the tracking detectors, while the energy measurements for photons and neutral hadrons is performed with the calorimetric system. The crucial step of the particle flow algorithm is to assign the correct calorimeter hits to reconstructed particles, requiring efficient separation of nearby showers.

Measurements of jet fragmentation at LEP have provided detailed information on the particle composition of jets (e.g. [3, 4]). On average, after the decay of short-lived particles, roughly 62% of the energy of jets is carried by charged particles (mainly hadrons), around 27% by photons, about 10% by long-lived neutral hadrons (e.g. n/K_L^0), and around 1.5% by neutrinos. Assuming calorimeter resolutions of $\sigma_E/E = 0.15/\sqrt{E(\text{GeV})}$ for photons and $\sigma_E/E = 0.55\sqrt{E(\text{GeV})}$ for hadrons, a jet energy resolution of $0.19/\sqrt{E(\text{GeV})}$ is obtained with the contributions from tracks, photons and neutral hadrons shown in Tab. I. In practice it is not possible to reach this level of performance for two main reasons. Firstly, particles travelling at small angles to the beam axis will not be detected. Secondly, and more importantly, it is not possible to perfectly associate all energy deposits with the correct particles. For example, if a photon is not resolved from a charged hadron shower, the photon energy is not counted. Similarly, if some of the energy from a charged hadron is identified as a separate cluster the energy is effectively double-counted. This *confusion* degrades particle flow performance. The crucial aspect of particle flow is the ability to correctly

* To appear in Proceedings of LCWS06, Bangalore, India, March 2006.

assign calorimeter energy deposits to the correct reconstructed particles. This places stringent requirements on the granularity of electromagnetic and hadron calorimeters. Consequently, particle flow performance is one of the main factors driving the overall ILC detector design. It should be noted that the jet energy resolution obtained for a particular detector concept is the combination of the intrinsic detector performance and the performance of the PFA software.

Component	Detector	Energy Fraction	Energy Res.	Jet Energy Res.
Charged Particles (X^\pm)	Tracker	$\sim 0.6 E_{\text{jet}}$	$10^{-4} E_{X^\pm}^2$	$< 3.6 \times 10^{-5} E_{\text{jet}}^2$
Photons (γ)	ECAL	$\sim 0.3 E_{\text{jet}}$	$0.15 \sqrt{E_\gamma}$	$0.08 \sqrt{E_{\text{jet}}}$
Neutral Hadrons (h^0)	HCAL	$\sim 0.1 E_{\text{jet}}$	$0.55 \sqrt{E_{h^0}}$	$0.17 \sqrt{E_{\text{jet}}}$

TABLE I: Contributions from the different particle components to the jet-energy resolution (all energies in GeV). The table lists the approximate fractions of charged particles, photons and neutral hadrons in a jet and the assumed single particle energy resolution.

III. THE PANDORAPFA PARTICLE FLOW ALGORITHM

PANDORAPFA[5] is a C++ implementation of a PFA algorithm running in the MARLIN[6, 7] framework. It was designed to be sufficiently generic for ILC detector optimisation studies and was developed and optimised using events generated with the MOKKA[8] program, which provides a GEANT4[9] simulation of the Tesla TDR[10] detector concept. The PANDORAPFA algorithm performs both calorimeter clustering and particle flow in a single stage. The algorithm has six main stages:

- i) **Tracking:** for the studies presented in this paper, the track pattern recognition is performed using Monte Carlo information[6]. The track parameters are then extracted using a helical fit. The projections of tracks onto the front face of the electromagnetic calorimeter are calculated using helical fits (which do not take into account energy loss along the track). Neutral particle decays resulting in two charged particle tracks (V^0 's) are identified by searching for pairs of tracks which do not originate from the interaction point and that are consistent with coming from a single point in space. Kinked tracks from charged particle decays to a single charged particle and a number of neutrals are also identified. When a kink is identified the parent track is usually removed for the purposes of forming the reconstructed particles.
- ii) **Calorimeter Hit Selection and Ordering:** isolated hits, defined on the basis of proximity to other hits, are removed from the initial clustering stage. The remaining hits are ordered into *pseudo-layers* which follow the detector geometry so that particles propagating outward from the interaction region will cross successive pseudo-layers. In most of the calorimeter the pseudo-layers follow the physical layers of the calorimeters except in the barrel-endcap overlap region and where the ECAL stave structure[10] results in low numbered layers which are far from the front face of the calorimeter. The assignment of hits to pseudo-layers removes the dependence of the algorithm on the explicit detector geometry whilst following the actual geometry as closely as possible. Within each pseudo-layer hits are ordered by decreasing energy.
- iii) **Clustering:** the main clustering algorithm is a forward projective method working from innermost to outermost pseudo-layer. In this manner hits are added to clusters or are used to seed new clusters. Throughout the clustering algorithm clusters are assigned a direction (or directions) in which they are growing. The algorithm starts by *seeding* clusters using the projections of reconstructed tracks onto the front face of the calorimeter. The initial direction of a track-seeded cluster is obtained from the track direction. The hits in each subsequent pseudo-layer are then looped over. Each hit, i , is compared to each clustered hit, j , in the previous layer. The vector displacement, \mathbf{r}_{ij} , is calculated and is used to calculate the parallel and perpendicular displacement of the hit with respect to the unit vector(s) $\hat{\mathbf{u}}$ describing the cluster propagation direction(s), $d_{\parallel} = \mathbf{r}_{ij} \cdot \hat{\mathbf{u}}$ and $d_{\perp} = |\mathbf{r}_{ij} \times \hat{\mathbf{u}}|$. Associations are made using a cone-cut, $d_{\perp} < d_{\parallel} \tan \alpha + \beta D_{\text{pad}}$, where α is the cone half-angle, D_{pad} is the size of a sensor pixel in the layer being considered, and β is the number of pixels added to the cone radius. Different values of α and β are used for the ECAL and HCAL with the default values set to $\{\tan \alpha_E = 0.3, \beta_E = 1.5\}$, and $\{\tan \alpha_H = 0.5, \beta_H = 2.5\}$ respectively. Associations may be made with hits in the previous 3 layers. If no association is made, the hit is used to seed a new cluster. This procedure is repeated sequentially for the hits in each pseudo-layer (working outward from ECAL front-face).
- iv) **Topological Cluster Merging:** by design the initial clustering errs on the side of splitting up true clusters rather than clustering energy deposits from more than one particle. The next stage of the algorithm is to merge clusters from tracks and hadronic showers which show clear topological signatures of being associated. A number of track-like and shower-like topologies are searched for including looping minimum ionising tracks, back-scattered

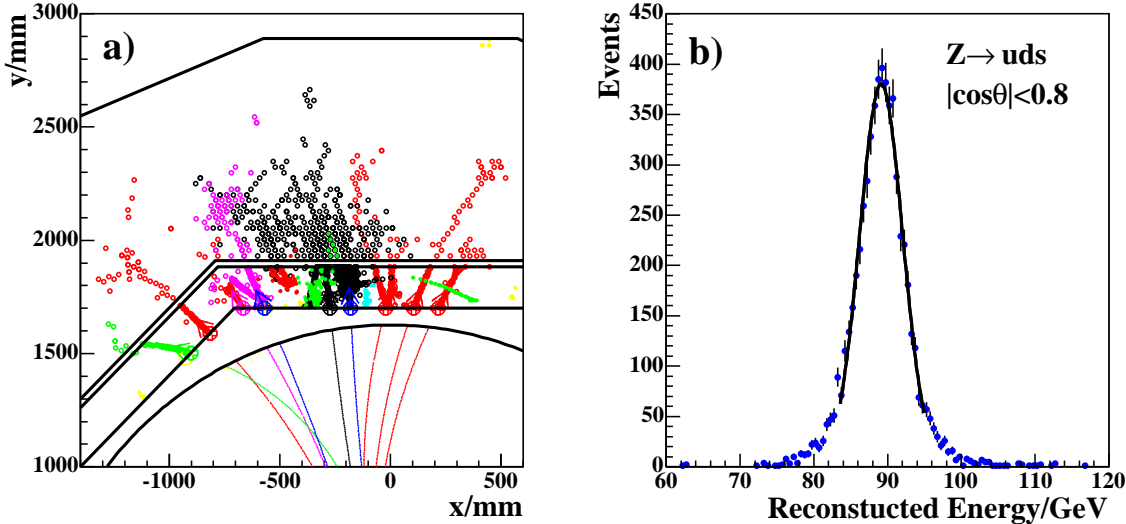


FIG. 1: a) PANDORAPFA reconstruction of a 100 GeV jet in the MOKKA simulation of the Tesla TDR detector. b) The total reconstructed energy from reconstructed PFOs in $Z \rightarrow u\bar{u}$ events for initial quark directions within the polar angle acceptance $|\cos \theta_{q\bar{q}}| < 0.8$. The solid line shows a Gaussian fit to the peak region with a standard deviation of 2.9 GeV.

tracks and showers associated with a hadronic interaction. Before clusters are merged, a simple cut-based photon identification procedure is applied. The cluster merging algorithms are only applied to clusters which have not been identified as photons.

v) Statistical Re-clustering: The previous four stages of the algorithm were found to perform well for 50 GeV jets. However, at higher energies the performance degrades rapidly due to the increasing overlap between hadronic showers from different particles. To address this, temporary associations of tracks with reconstructed calorimeter clusters are made. If the track momentum is incompatible with the energy of the associated cluster re-clustering is performed. If $E_{\text{CAL}} - E_{\text{TRACK}} > 3.5\sigma_E$, where σ_E is the energy resolution of the cluster, the clustering algorithm, described in *iii*) and *iv*) above, is reapplied to the hits in that cluster. This is repeated, using successively smaller values of the α s and β s in the clustering finding algorithm (stage *iii*)) until the cluster splits to give an acceptable track-cluster energy match. Similarly, if $E_{\text{TRACK}} - E_{\text{CAL}} > 3.5\sigma_E$ the algorithm attempts to merge additional clusters with the cluster associated with the track. In doing so high energy clusters may be split as above.

vi) Formation of Particle Flow Objects: The final stage of the algorithm is to create Particle Flow Objects (PFOs) from the results of the clustering. Tracks are matched to clusters on the basis of the distance closest approach of the track projection into the first 10 layers of the calorimeter. If a hit is found within 50 mm of the track extrapolation an association is made. The reconstructed PFOs are written out in LCIO[6] format.

IV. PERFORMANCE

Fig. 1a) shows an example of a PANDORAPFA reconstruction of a 100 GeV jet from a $Z \rightarrow u\bar{u}$ decay at $\sqrt{s} = 200$ GeV. The ability to track particles in the high granularity Tesla TDR calorimeter can be seen clearly. Fig. 1b) shows the total PFA reconstructed energy for $Z \rightarrow u\bar{u}$ events with $|\cos \theta_{q\bar{q}}| < 0.8$, where $\theta_{q\bar{q}}$ is the polar angle of the generated $q\bar{q}$ system. These events were generated at $\sqrt{s} = 91.2$ GeV using the Tesla TDR detector model. The root-mean-square deviation from the mean (rms) of the distribution is 4.0 GeV. However, quoting the rms as a measure of the performance over-emphasises the importance of the tails. For example, in this figure, the central peak is well described by a Gaussian of width 2.9 GeV, equivalent to a resolution of $\sigma_E/E = 0.31/\sqrt{E(\text{GeV})}$. In this paper two measures of the performance are quoted. The first measure, rms_{90} , is the rms in the smallest range of reconstructed energy which contains 90 % of the events. The second performance measure is obtained from a fit to the reconstructed energy distribution. The fit function is the sum of two Gaussian distributions with a common mean but different widths. The width of the narrower Gaussian, which is constrained to contain 75 % of the events, gives a measure of the resolution in the peak, σ_{75} . For the data shown in Fig. 1b) both methods give a resolution

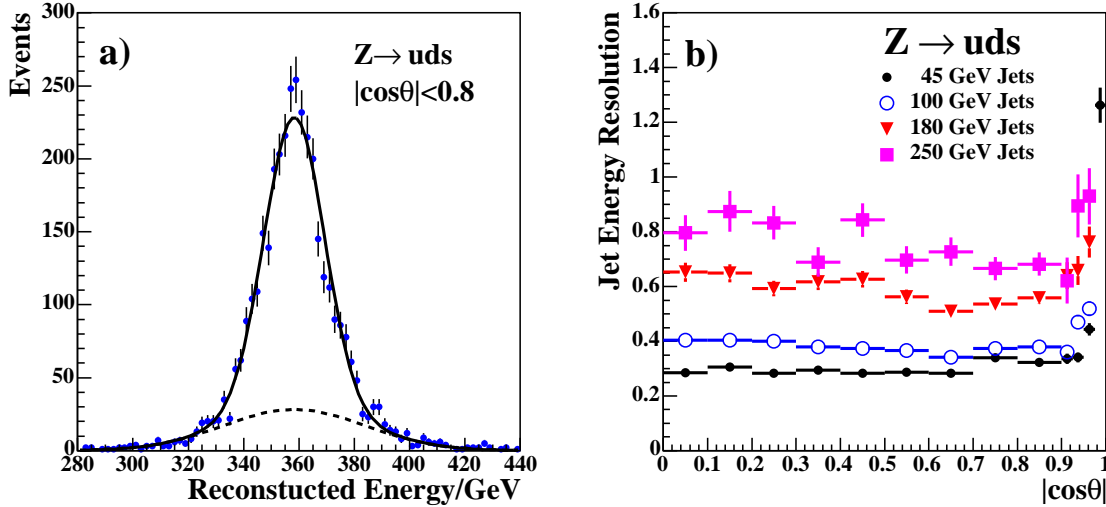


FIG. 2: a) The total reconstructed energy from reconstructed PFOs in $Z \rightarrow \text{uds}$ at $\sqrt{s} = 360$ GeV for initial quark directions within the polar angle acceptance $|\cos \theta| < 0.8$. The solid line shows a results of the fit to two Gaussians and the dashed line indicates the contribution from the broader Gaussian which is constrained to contain 25 % of the events. b) The jet energy resolution, defined as the α in $\sigma_E/E = \alpha\sqrt{E(\text{GeV})}$, plotted versus $\cos \theta_{q\bar{q}}$ for four different values of \sqrt{s} .

of $\sigma_E/E = 0.3/\sqrt{E(\text{GeV})}$; the ILC goal. However, this is of little consequence to ILC physics where, in general, the jets will be higher in energy.

The majority of interesting ILC physics will consist of final states with at least six fermions, setting a “typical” energy scale for ILC jets as approximately 85 GeV and 170 GeV at $\sqrt{s} = 500$ GeV and $\sqrt{s} = 1$ TeV respectively. Fig. 2a shows the reconstructed total energy in $Z \rightarrow \text{uds}$ events (generated without ISR or beamstrahlung effects) at $\sqrt{s} = 360$ GeV. The fit to the sum of a double Gaussian gives $\sigma_{75} = 10.8$ GeV, equivalent to a resolution of $\sigma_E/E = 0.57/\sqrt{E(\text{GeV})}$, significantly worse than that obtained for lower energy jets. Fig. 2 shows the jet energy resolution for $Z \rightarrow \text{uds}$ events plotted against $|\cos \theta_{q\bar{q}}|$ for four different values of \sqrt{s} .

V. DISCUSSION

The results described above are summarised in Tab. II. The observed jet energy resolution in simulated events is not described by the expression $\sigma_E/E = \alpha/\sqrt{E(\text{GeV})}$. This is not surprising, as the particle density increases it becomes harder to correctly associate the calorimetric energy deposits to the particles and the confusion term increases. Empirically it is found that the total energy resolutions in Tab. II can be described by a jet energy resolution of $\sigma_E/E = 0.265/\sqrt{E(\text{GeV})} + 1.2 \times 10^{-4}E(\text{GeV})$, where E is the jet energy. This expression represents the current performance of the PANDORAPFA algorithm and should not be considered as anything more fundamental. It should be noted that in the current MOKKA simulation of the Tesla TDR detector the muon chambers are not included. In principle these can be used as a “tail-catcher” to improve the energy measurement for high energy hadronic showers which may not be fully contained in the HCAL. In the current version of PANDORAPFA no attempt is made to correct for this energy leakage. It is noticeable in Fig. 2b that the energy resolution improves with increasing polar angle in the barrel region of the detector, possibly due to increasing shower containment.

Jet Energy	rms_{90} $\text{rms}_{90}/\sqrt{E(\text{GeV})}$		σ_{75} $\sigma_{75}/\sqrt{E(\text{GeV})}$	
	45 GeV	100 GeV	180 GeV	250 GeV
45 GeV	2.8 GeV	0.30	2.8 GeV	0.30
100 GeV	5.3 GeV	0.38	5.2 GeV	0.37
180 GeV	11.0 GeV	0.58	10.8 GeV	0.57
250 GeV	16.8 GeV	0.76	16.8 GeV	0.75

TABLE II: Jet energy resolution, expressed as both rms_{90} and σ_{75} , for $Z \rightarrow \text{uds}$ events with $|\cos \theta_{q\bar{q}}| < 0.8$.

VI. CONCLUSIONS

Particle flow calorimetry is widely believed to be the key to reaching the ILC jet energy resolution goal of $\sigma_E/E = 0.3/\sqrt{E(\text{GeV})}$. Consequently, the design and optimisation of detectors for the ILC depends both on hardware and on sophisticated software reconstruction. For the Tesla TDR detector concept, the PANDORAPFA particle flow algorithm achieves good performance, $< 0.4/\sqrt{E(\text{GeV})}$, for jet energies upto about 100 GeV. For higher energies the performance degrades significantly reaching the equivalent of $0.6/\sqrt{E(\text{GeV})}$ for 200 GeV jets. With further optimisation of the algorithm the performance is expected to improve. However, the current algorithm is adequate for most ILC physics studies at $\sqrt{s} = 500$ GeV and may be used for the optimisation of the design of the ILC detector(s).

- [1] M. A. Thomson, Proc. of EPS-HEP 2003, Aachen. Topical Vol. of Eur. Phys. J. C Direct (2004).
- [2] ALEPH Collaboration, D. Buskulic et al., Nucl. Inst. Meth. **A360** (1995) 481.
- [3] I.G. Knowles and G.D. Lafferty, J. Phys. **G23** (1997) 731.
- [4] M. G. Green, S. L. Lloyd, P. N. Ratoff and D. R. Ward, “Electron-Positron Physics at the Z”, IoP Publishing (1998).
- [5] <http://www.hep.phy.cam.ac.uk/~thomson/pandoraPFA/>.
- [6] <http://www-flc.desy.de/ilcsoft/ilcsoftware/>.
- [7] O. Wendt, “Marlin and MarlinReco”, to appear in Proc. of LCWS06, Bangalore, March 2006.
- [8] <http://polywww.in2p3.fr/activites/physique/geant4/tesla/www/mokka/>.
- [9] GEANT4 collaboration, S. Agostinelli et al., Nucl. Instr. and Meth. **A506** (2003) 3;
GEANT4 collaboration, J. Allison et al., IEEE Trans. Nucl. Sci. 53 (2006) 1.
- [10] TESLA Technical Design Report, DESY 2001-011, ECFA 2001-2009 (2001).